

# Production of $B_c$ mesons in photon–photon and hadron–hadron collisions<sup>1</sup>

Karol Kołodziej<sup>a,2,3</sup>, Arnd Leike<sup>b,2</sup> and Reinhold Rückl<sup>b,c,2</sup>

<sup>a</sup>*Institute of Physics, University of Silesia,  
PL-40007 Katowice, Poland*

<sup>b</sup>*Sektion Physik der Universität München,  
Theresienstr. 37, D-80333 München, FRG*

<sup>c</sup>*Max-Planck-Institut für Physik, Werner-Heisenberg-Institut,  
Föhringer Ring 6, D-80805 München, FRG*

## Abstract

We discuss two-photon and hadronic production of  $B_c$  mesons in nonrelativistic bound state approximation and to lowest order in the coupling constants  $\alpha$  and  $\alpha_s$ . It is shown that in photon-photon collisions, heavy quark fragmentation is dominated by recombination of  $\bar{b}$  and  $c$  quarks up to the highest accessible transverse momenta. In contrast, in hadroproduction, which at high energies mainly involves gluon–gluon collisions, the fragmentation mechanism dominates at transverse momenta  $p_T > m_{B_c}$ , providing a simple and satisfactory approximation of the complete  $O(\alpha_s^4)$  results in the high- $p_T$  regime. Contradictions in previous publications on hadroproduction of  $B_c$  mesons are clarified. We also present predictions for cross sections and differential distributions at present and future accelerators.

---

<sup>1</sup>Talk presented by K. Kołodziej at The Second German-Polish Symposium “*New Ideas in the Theory of Fundamental Interactions*”, Zakopane, Poland, 11–15 September, 1995.

<sup>2</sup>Supported by the German Federal Ministry for Research and Technology BMBF under contract 05 6MU93P, and by the EC-program HCM under contract CHRX-CT93-0132

<sup>3</sup>Supported by the Polish Ministry of Education under contract No. PB 659/P03/95/08

Since the top quark is too short lived for the formation of quarkonium-like resonances,  $B_c$  mesons are most probably the only flavoured heavy quark resonances in nature. Because of flavour conservation in strong and electromagnetic interactions, the  $B_c$  ground state must decay weakly. The nonrelativistic nature of these bound states provides unique possibilities to compute genuine nonperturbative quantities such as fragmentation functions and weak matrix elements, and to study interesting aspects of the strong and weak dynamics of hadrons.

A limit on  $B_c$  production has been reported recently by the CDF-collaboration at the Tevatron [1]. At the LHC, the production rates are predicted to be large enough for a detailed study of the production and decay properties [2]. Also at linear colliders in the TeV energy range,  $B_c$  mesons produced in collisions of Compton or bremsstrahlung photons may come into experimental reach [3].

In this talk, we report about two recent studies [2, 3] of  $B_c$  production. We discuss the fragmentation and recombination mechanisms and compare the relative importance of them in photon-photon and hadron-hadron collisions. As a main result, we clarify quantitatively the validity of the hard scattering description in terms of heavy quark fragmentation functions. Furthermore, on the basis of two completely independent calculations, we resolve contradictions in previous publications on hadronic production of  $B_c$  mesons [4]–[7]. Finally, we present the most relevant integrated cross sections and differential distributions as predicted in lowest-order perturbation theory and nonrelativistic bound state approximation.

In photon-photon collisions,  $B_c$  mesons are produced in association with  $b$ - and  $\bar{c}$ -quark jets:

$$\gamma\gamma \rightarrow B_c b \bar{c}. \quad (1)$$

This is also the case in hadronic collisions, where gluon-gluon scattering,

$$gg \rightarrow B_c b \bar{c}, \quad (2)$$

is the dominant subprocess at high energies. In general, one can distinguish two production mechanisms, namely heavy quark fragmentation and recombination. We have found these mechanisms to contribute quite differently in the two reactions, which makes a comparison very interesting.

The twenty  $O(\alpha^2\alpha_s^2)$  Feynman diagrams of process (1) can be classified in three gauge invariant subsets characterized in Fig. 1: subset (I<sub>b</sub>) with the  $b$ -quark line coupled to the primary photons, subset (I<sub>c</sub>) with the  $c$ -quark line coupled to the primary photons, and subset (II) with the  $b$ -quark line coupled to one of the primary photons and the  $c$ -quark line to the other one. The three subsets can be interpreted physically as describing, respectively,  $b\bar{b}$  production and subsequent  $\bar{b}$  fragmentation,  $\bar{b} \rightarrow B_c \bar{c}$ ,  $c\bar{c}$  production and subsequent  $c$  fragmentation,  $c \rightarrow B_c b$ , and simultaneous production of a  $b\bar{b}$  and  $c\bar{c}$  pair and recombination of the  $\bar{b}$ - and  $c$ -quark into a  $B_c$  meson. The gluon-fusion process (2) involves a larger number of Feynman diagrams because of the presence of the gluon self-coupling. To  $O(\alpha_s^4)$ , one has thirty-six diagrams in total. More importantly, they cannot be divided up in gauge invariant subsets corresponding to the production mechanisms typified in Fig. 1.

In the following, we concentrate on the production of the pseudoscalar ( $B_c$ ) and vector ( $B_c^*$ ) bound states. Furthermore, we consider the nonrelativistic limit, in which the relative momentum of the constituents and their binding energy are neglected relative to the  $b$ - and  $c$ -quark

masses. In this limit, the masses of the bound states are equal to the sum of  $m_b$  and  $m_c$ , and the momenta of both constituent quarks are proportional to the bound state momentum. Moreover, the amplitudes for the production of  $S$ -waves factorize into hard scattering amplitudes for  $\gamma\gamma$  (or  $gg$ )  $\rightarrow b\bar{b}c\bar{c}$  times the  $S$ -wave function at the origin. The latter can be related to the  $B_c^{(*)}$  decay constants. All this results in the simple substitution rule [8, 3, 2]

$$v(p_{\bar{b}})\bar{u}(p_c) = \frac{f_{B_c^{(*)}}}{\sqrt{48}}(\not{p} - M)\Pi_{SS_Z}, \quad (3)$$

indicated in Fig. 1 by the black blob, where  $v(p_{\bar{b}})$  and  $\bar{u}(p_c)$  denote the  $\bar{b}$ - and  $c$ -quark spinors, respectively, and  $\Pi_{SS_Z} = \gamma_5(\not{\epsilon})$  is the spin projector for  $B_c$  ( $B_c^*$ ). Note that the colour structure is not accounted for in Eq. (3).

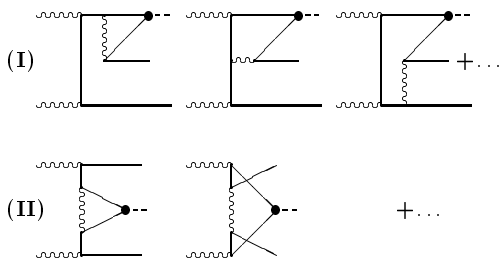


**Fig. 1.** Characteristic topologies of the lowest-order Feynman diagrams contributing to  $\gamma\gamma \rightarrow B_c b\bar{c}$ .

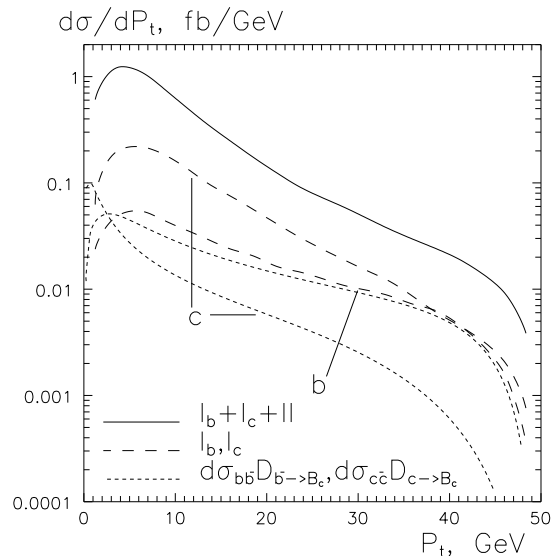


**Fig. 2.** Transverse momentum distributions of  $B_c$  mesons produced in  $\gamma\gamma \rightarrow B_c b\bar{c}$  at  $\sqrt{s} = 100$  GeV for the different production mechanisms and approximations described in the text.

The squared matrix elements for the processes (1) and (2) have been calculated independently using two different methods, the traditional trace technique and the method of helicity amplitudes. The results are found to be in perfect agreement. In addition, we have checked external gauge invariance, that is the vanishing of the matrix elements when the polarization vector of any of the initial photons or gluons is substituted by its momentum. For process (1), we have also tested internal gauge invariance, that is the independence of the matrix element of the gauge parameter in the gluon propagator. Finally, we have double-checked the phase space integration using two different Monte Carlo routines. For more details of the calculation we refer to refs. [2] and [3].

In addition to the above  $O(\alpha^2\alpha_s^2)$  and  $O(\alpha_s^4)$  calculations, we have also studied the factorized description of the processes (1) and (2) in terms of  $b\bar{b}(c\bar{c})$  production followed by  $\bar{b}(c)$

fragmentation [12]:

$$d\sigma_{B_c} = d\sigma_{b\bar{b}} \otimes D_{\bar{b} \rightarrow B_c \bar{c}}(z) \quad (d\sigma_{c\bar{c}} \otimes D_{c \rightarrow B_c b}(z)). \quad (4)$$

The relevant fragmentation functions  $D_{\bar{b}}(z)$  and  $D_c(z)$  have been derived from perturbation theory [9]. They are known to provide a perfect approximation of the energy distribution  $d\sigma/dz$  in  $e^+e^- \rightarrow B_c \bar{c}b$  [9, 10] in order  $\alpha_s^2$ . Clearly, in photon-photon and hadron-hadron production such a factorized description cannot be expected to work close to threshold and at small  $p_T$ , where the quark masses play a role. The question is how well this approximation works at high- $p_T$ . Previous studies of this issue only give qualitative and partly contradicting answers [4, 6]. This motivated us to compare the factorized approximation (4) with our complete lowest-order calculations, and to determine the region of validity of (4) quantitatively.

The numerical results plotted in Figs. 2-6 have been obtained with the following values of the parameters:

$$m_b = 4.8 \text{ GeV}, \quad m_c = 1.5 \text{ GeV}, \quad \alpha = 1/129, \quad f_{B_c} = f_{B_c^*} = 0.4 \text{ GeV} \quad [11]. \quad (5)$$

Furthermore, we have used the running coupling constant  $\alpha_s(Q^2)$  in leading logarithmic approximation for five flavours and normalized to  $\alpha_s(m_Z^2) = 0.113$ . Additional specifications are given when needed.

Fig. 2 illustrates transverse momentum distributions of the  $B_c$  in  $\gamma\gamma$ -production (1). We see that the description (4) in terms of  $b\bar{b}$  production and  $\bar{b}$ -fragmentation and the corresponding subset ( $I_b$ ) of the diagrams of Fig. 1 give distributions (dotted and dashed curves, respectively, labeled by  $b$ ) which are very similar in shape and normalization except in the low- $p_T$  region, where the factorized approximation is expected to break down. As far as the shape is concerned this is also true for  $c\bar{c}$  production and  $c$  fragmentation (curves labeled by  $c$ ). However, in this case the approximation (4) fails to reproduce the correct magnitude of the cross section predicted by the diagrams subset ( $I_c$ ) of Fig. 1. Note that primary  $c$ -quark production is enhanced to  $b$ -quark production by a factor 16 due to the ratio  $(Q_c/Q_b)^4$  of the electric charges. On the other hand, the radiation of a  $c\bar{c}$ -pair from a  $b$ -quark leads to a harder  $p_T$  spectrum for the  $B_c$  bound states than the radiation of a  $b\bar{b}$ -pair from  $c$ -quarks. Finally, the most important observation is that the recombination mechanism, represented by the diagrams (II) of Fig. 1, dominates  $B_c$  production not only at low  $p_T$ , as one could have expected, but also in the high- $p_T$  region up to the kinematical limit. In other words, the familiar description of high- $p_T$  hadron production in terms of the production and fragmentation of quarks is inadequate for single  $B_c$  production in  $\gamma\gamma$ -scattering.

The main features of the transverse momentum distributions of the  $B_c$  produced in the subprocess  $gg \rightarrow B_c b\bar{c}$  are illustrated in Fig. 3. Here, we see that the fragmentation description (4) indeed approaches the  $p_T$ -distributions resulting from the complete  $O(\alpha_s^4)$  calculation, but only in the tails of the distributions. In order to demonstrate the effect of the quark masses on the fragmentation kinematics, we have assumed three different relations between daughter and parent momenta:

$$p_T = z\sqrt{\hat{s}/4 - \mu^2} \sin \theta_b, \quad p_L = p_T \cot \theta_b, \quad \mu = M \text{ (I)}, \quad m_b \text{ (II)}, \quad 0 \text{ (III)}, \quad (6)$$

where  $\sqrt{\hat{s}}$  is the gluon-gluon c.m. energy. Case I obeys the physical phase space boundaries. The choices II and III have been considered in refs. [12] and [13], respectively. Fig. 3 shows

that the mass ambiguities of the fragmentation approach increase as  $\hat{s}$  decreases and that they become non-negligible at  $\sqrt{\hat{s}} \leq 40$  GeV. Comparing the approximations with the  $O(\alpha_s^4)$  results, one observes a slight preference for choice I or II. Most interesting, however, is the difference to  $\gamma\gamma \rightarrow B_c b\bar{c}$  where heavy quark fragmentation is completely subdominant even at large  $p_T$ . Apparently, the presence of the gluon self-coupling and colour factors has a drastic influence on the relative importance of the fragmentation and recombination.

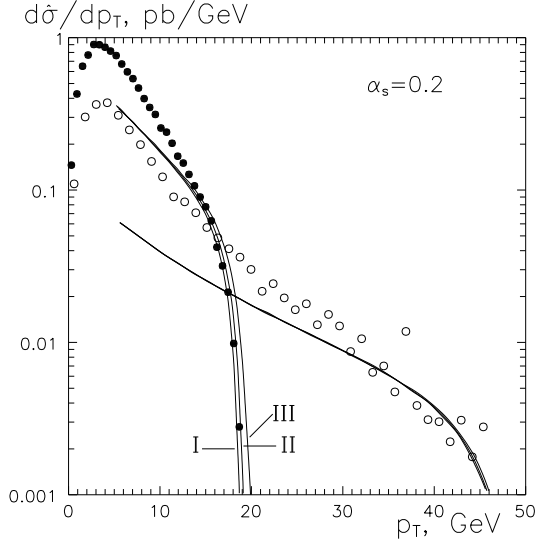


**Fig. 3.** Transverse momentum distributions of  $B_c$  mesons produced in  $gg \rightarrow B_c b\bar{c}$  at  $\sqrt{\hat{s}} = 40$  and 100 GeV: complete  $O(\alpha_s^4)$  calculation (circles) and approximation eq. (4) (solid curves). The labels I–III refer to the kinematics specified in eq. (6).

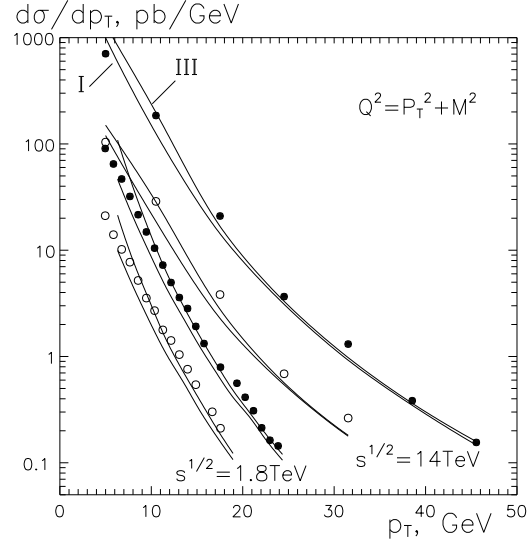


**Fig. 4.** Transverse momentum distribution of the  $B_c$  in  $p\bar{p}(pp)$  collisions at the Tevatron (LHC) energies: complete  $O(\alpha_s^4)$  calculation (circles) and fragmentation approximation eq. (4) (solid curves). The labels I and III refer to the kinematics eq. (6). Results are shown without a rapidity cut (full circles) and for  $|y| \leq 0.5$  (empty circles).

Predictions for the  $p_T$  distributions of  $B_c$  mesons in  $p\bar{p}$  and  $pp$  collisions at Tevatron and LHC energies are obtained by convoluting the  $gg$ -subprocess distributions with the MRS(A') gluon structure functions [14]. The results with and without cuts in rapidity are plotted in Fig. 4 and compared with the fragmentation approximation. We have assumed the scale  $Q^2 = p_T^2 + M^2$  in both  $\alpha_s(Q^2)$  and the structure functions. The evolution effects in the fragmentation function  $D_b(z)$  are ignored for consistency. These effects are studied in ref. [12]. We see that after convolution the  $O(\alpha_s^4)$  calculation and the fragmentation description (4) are in reasonable agreement at  $p_T \geq 10$  GeV. This can be understood from the properties of the unfolded  $p_T$ -distributions illustrated in Fig. 3 and from the rise of the gluon density at small  $x$  which favours contributions from the smallest possible subenergies  $\hat{s}$ , and hence from the tails of the spectra. With decreasing  $p_T$ , the fragmentation picture gradually breaks down and at  $p_T < 5$  GeV only the complete  $O(\alpha_s^4)$  calculation makes sense. Furthermore, the sensitivity to the kinematical prescription (6) decreases slowly with increasing  $p_T$ .

The total hadronic cross sections for  $B_c$  and  $B_c^*$  production are shown in Fig. 5. The typical rise of  $\sigma$  with energy is due to the rise of the gluon density as  $x$  approaches  $x_{min}$  and the peaking of  $\hat{\sigma}$  near threshold. In order to demonstrate the scale dependence of  $\sigma$ , we have indicated the  $B_c$  cross sections at  $\sqrt{s} = 0.1, 1$  and 10 TeV for different choices of  $Q^2$ . As one can see, at lower energies, the notorious scale ambiguity of leading logarithmic approximations leads to an uncertainty of more than one order of magnitude. Only at very high energies, the uncertainty shrinks to a factor two. It is interesting to note that the differences in the predictions resulting from different parametrizations of the gluon density, e.g. CTEQ2 [15] instead of MRS(A') [14], would be invisible in Fig. 5. Other uncertainties, connected with the decay constants  $f_{B_c^{(*)}}$  and the effective quark masses  $m_b$  and  $m_c$ , amount at least to another factor of two.

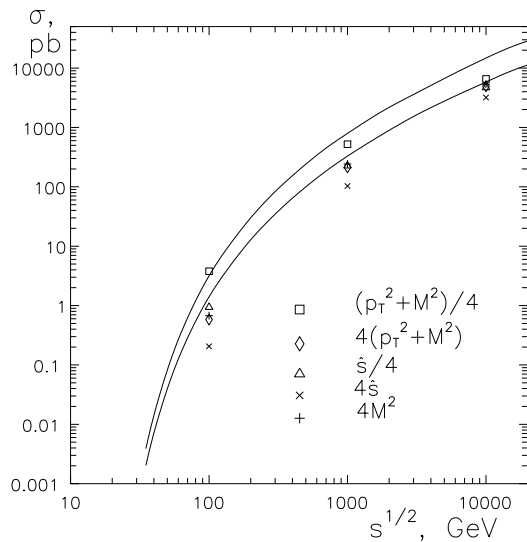


**Fig. 5.** Total cross sections for  $pp(p\bar{p}) \rightarrow B_c^{(*)} b\bar{c} + X$  versus the c.m. energy. The lower (upper) curve show the predictions for  $B_c$  ( $B_c^*$ ) and the scale  $Q^2 = p_T^2 + M^2$ . The symbols indicate expectations for other choices of  $Q^2$ .

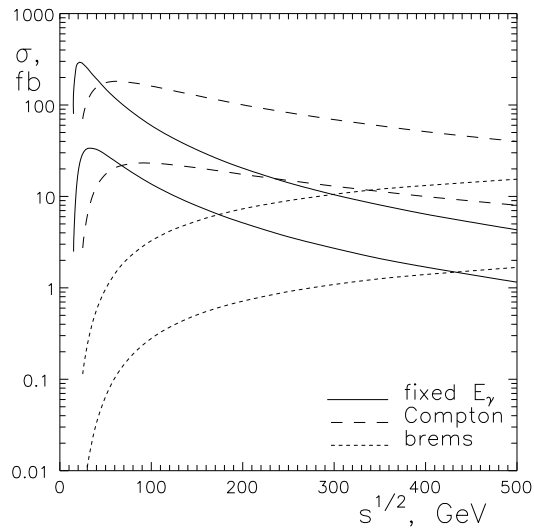


**Fig. 6.** Total cross sections for  $\gamma\gamma \rightarrow B_c^{(*)} b\bar{c}$  versus fixed  $\gamma\gamma$  c.m. energy, and after convolution with Compton and bremsstrahlung spectra, versus the  $e^+e^-$  c.m. energy. The lower (upper) curves correspond to  $B_c$  ( $B_c^*$ ) production. The scale of  $\alpha_s$  is chosen to be  $p_T^2 + M^2$ .

The second main motivation for our own studies, besides examining the validity of the factorized fragmentation approach, has been the wish to resolve the confusion created by previous calculations [4] – [7] of hadroproduction of  $B_c$  mesons which have contradicted each other. Because of the ambiguities and uncertainties pointed out above, comparison was not always easy. We have been very careful in adjusting parameters and the gluon density to the choice in the respective calculation we considered. We also focused as much as possible on the comparison of  $gg$  cross sections and distributions being most transparent. In cases where  $gg$  results were not given, we compared the convoluted cross sections. The outcome of this comparison was surprising. As described in detail in ref. [2], we were not able to reproduce any of the previous numerical predictions. In the meantime, the authors of ref. [4] revised their work [16] and now agree with our results. Also the authors of [6] corrected a normalization error in

[13] (this paper appeared almost simultaneously with [7]), so that the  $gg$  cross section coincide with what we found except at very high energies. However, the  $p_T$  distributions given in [13] still disagree substantially with ours.

In order to evaluate the observability of  $B_c$  mesons at the Tevatron and LHC, it is useful to integrate the  $p_T$ -distributions of Fig. 4 over  $p_T \geq p_T^{min}$ . Assuming an integrated luminosity of  $100 \text{ pb}^{-1}$ , one can expect about  $10^4$   $B_c$  mesons with  $p_T^{min} = 10 \text{ GeV}$  at the Tevatron, without taking into account contributions from the production and decay of  $B_c^*$  mesons and heavier states. This rate should be sufficient for discovery in the channel  $B_c \rightarrow J/\psi X$ , for which a branching ratio of the order of 10% is predicted [17]. In fact, first results of such a search have already been reported in [1]. Finally, at the LHC for  $100 \text{ fb}^{-1}$ , one can expect  $10^7$  direct  $B_c$  mesons at  $p_T^{min} = 20 \text{ GeV}$ . This rate should then allow a more detailed study of production and decay properties.

Predictions on the production rates of  $B_c$  mesons in photon-photon collisions at future  $e^+e^-$  machines are obtained by folding the total cross sections for  $\gamma\gamma \rightarrow B_c^{(*)}b\bar{c}$  with the photon spectrum generated by Compton back-scattering of high intensity laser light on  $e^\pm$  beams [18], or with the Weizsäcker–Williams bremsstrahlung spectrum [19]. The expectations are illustrated in Fig. 6, where we have plotted the convoluted cross sections for  $B_c$  and  $B_c^*$  production versus the  $e^+e^-$  centre-of-mass energy, together with the unfolded cross sections as a function of fixed  $\gamma\gamma$  centre-of-mass energy. Because of the long soft tail of the Compton spectrum, and the shape of the  $\gamma\gamma$  cross section which peaks just above threshold, the convolution increases the cross sections substantially for energies above 100 GeV. At a 500 GeV linear collider and for an integrated luminosity of  $10 \text{ fb}^{-1}$ , one can produce about 100  $B_c$  and 400  $B_c^*$ . The yield of  $B_c$  mesons from bremsstrahlung photons is invisibly small at LEP energies, but increases logarithmically with energy. In the TeV energy range bremsstrahlung photons become competitive with back-scattered laser photons in producing  $B_c$  mesons. Although, the prospect of  $B_c$  physics in  $\gamma\gamma$  collisions are not very bright, observation of  $B_c$  mesons does not appear completely unfeasible.

## References

- [1] Abe et al., *A limit on  $\sigma Br(B_c^\pm \rightarrow J/\Psi + \pi^\pm)/\sigma Br(B_u^\pm \rightarrow J/\Psi + K^\pm)$  in  $\sqrt{s} = 1.8 \text{ TeV}$  proton – anti-proton collisions*, Fermilab-Conf-95-202-E.
- [2] K. Kołodziej, A. Leike, R. Rückl, Phys. Lett. **B 355** (1995) 337.
- [3] K. Kołodziej, A. Leike, R. Rückl, Phys. Lett. **B 348** (1995) 219.
- [4] C.-H. Chang, Y.-Q. Chen, Phys. Rev. **D48** (1993) 4086; C.-H. Chang, Y.-Q. Chen, G.-P. Han, H.-T. Jiang, AS-ITP-94-24, hep-ph/9408242.
- [5] S.R. Slabospitsky, IHEP 94-53, hep-th/9404346.
- [6] A.V. Berezhnoy, A.K. Likhoded, M.V. Shevlyagin, Phys. Atom. Nucl. **58** (1995) 672, hep-ph/9408284.
- [7] M. Masetti, F. Sartogo, Phys. Lett. **B357** (1995) 659, hep-ph/9503491.

- [8] B. Guberina, J.H. Kühn, R.D. Peccei, R. Rückl, Nucl. Phys. **B174** (1980) 317.
- [9] F. Amiri, C.-R. Ji, Phys. Lett. **B195** (1987) 593; C.-H. Chang, Y.-Q. Chen, Phys. Rev. **D46** (1992) 3845; E. Braaten, K. Cheung, T.C. Yuan, Phys. Rev. **D48** (1993) R5049.
- [10] A. Leike, R. Rückl, Nucl. Phys. **B** (Proc. Suppl.) **37B** (1994) 215.
- [11] S. Reinshagen, diploma thesis, Univ. of Munich, 1991; S. Reinshagen, R. Rückl, in Proc. of the Workshop on Quantum Field Theoretical Aspects of High Energy Physics, eds. B. Geyer, E.-M. Ilgenfritz, Univ. of Leipzig, 1993.
- [12] K. Cheung, Phys. Rev. Lett. **71** (1993) 3413; K. Cheung, T.C. Yuan, UCD-95-4, CPP-94-37, hep-ph/9502250.
- [13] A.V. Berezhnoy, A.K. Likhoded, O.P. Yushchenko, IHEP-95-59, hep-ph/9504302.
- [14] A.D. Martin, W.J. Stirling, R.G. Roberts, Phys. Lett. **B354** (1995) 155.
- [15] H.L. Lai et al., Phys. Rev. **D51** (1995) 4763.
- [16] C.-H. Chang, Y.-Q. Chen, G.-P., Han, H.-T. Jiang, IC/94/225, AS-ITP-94-24 revised version, June 1995.
- [17] D. Du, Z. Wang, Phys. Rev. **D39** (1989) 1342; M. Lusignoli, M. Masetti, Z. Phys. **C51** (1991) 549; V.V. Kiselev, A.K. Likhoded, A.V. Tkabladze, Phys. At. Nucl. **56**(1993) 643; Likhoded et al., Nucl. Instrum. Methods **A333** (1993) 209; P. Colangelo, G. Nardulli, N. Paver, Z. Phys. **C57** (1993) 43.
- [18] I.F. Ginzburg, G.L. Kotkin, V.I. Telnov, Nucl. Instr. Meth. **205** (1983) 47; V.I. Telnov, in Proc. of the IXth Int. Workshop on Photon-Photon Collisions, eds. D.O. Caldwell, H. P. Paar (World Scientific, Singapore, 1992) p. 369.
- [19] C. F. Weizsäcker, Z. Phys. **88** (1934) 612; E. J. Williams, Phys. Rev. **45** (1934) 729.